



Effect of left ventricular assist device on the hemodynamics of a patient-specific left heart

Vikas Kannojiya¹ · Arup Kumar Das¹ · Prasanta Kumar Das²

Received: 19 August 2021 / Accepted: 7 April 2022 / Published online: 20 April 2022
© International Federation for Medical and Biological Engineering 2022

Abstract

This article describes the numerical efforts made to investigate the influence of a left ventricular assist device (LVAD) on the patient-specific left heart's hemodynamics. Two different computational geometries with left heart have been simulated over the entire cardiac cycle (case 1: healthy heart without LVAD and case 2: diseased heart with LVAD). The blood flow was simulated by implementing Bird-Carreau non-Newtonian model. Simulation results show that implantation of LVAD pump imparts major influence on the hemodynamics of the heart; it also provides a cardiac output of 4.87 L/min even at the diastolic phase. Furthermore, post LVAD implantation, approximately eight times more wall shear stress, is noticed at the aorta during the ventricular systole. In particular, major changes in the fluidics are observed inside the aortic region. A possibility of flow stagnation is noticed near the aortic root during the diastolic phase due to the bisection of incoming bloodstreams from the outflow graft. The flow characteristics of the LVAD pump are also observed to be significantly different from the idealized simulations (idealized tubular inlet situation). The observation of this study can help in understanding post-implant critical hemodynamic issues due to pump performance and its subsequent impact on the heart.

Graphical abstract

A simulation approach-based study has been performed to investigate the influence of LVAD on the hemodynamics of a heart. A 3D computational model of a patient-specific heart has been created from CT scan datasets for diastole and systole phases (a). An axial flow blood pump has been implanted computationally into the left heart (b). The implanted blood pump enhances the cardiac output and elevates shear generation (c) and (d).

Keywords Left heart · Ventricle · Blood pump · LVAD · CFD

1 Introduction

Heart failure (HF) is a common disease, being suffered by many across the globe. In 2014, Ambrosy et al. [1] have reported that around 26 million peoples have suffered from heart failure, and the number is increasing in prevalence. Owing to the scarcity of heart donors, it is impossible to perform a heart transplant to treat every critical stage heart failure patient [2]. It is known that left-sided HF is the most common type [3], mainly occurred due to the weakened left

ventricle. A left ventricular assist device (LVAD) can support the functioning of such ventricles to maintain the cardiac circulations by delivering blood to the aorta and reduce mortality due to heart failure [4]. LVADs also reduce the dependency on donors for the treatment of heart patients requiring transplantation.

Though pulsatile LVADs have their own advantages [5], at present, continuous-flow LVADs are the most demanded one for implantation due to their compactness, reliability, and durability [6, 7]. It should be noted that LVADs have undergone tremendous design and technological improvements. But there is still scope of development in design of LVADs to diminish the existing patient-related complications [8]. To understand such complications, many numerical studies have been performed highlighting fluidics inside the heart [9–13]. On the other hand, several researches are also being conducted to evaluate LVAD pump performance for the

✉ Vikas Kannojiya
vkannojiya@me.iitr.ac.in

¹ Mechanical and Industrial Engineering Department, IIT Roorkee, Roorkee 247667, Uttarakhand, India

² Department of Mechanical Engineering, IIT Kharagpur, Kharagpur, West Bengal, India

development of new and advanced versions [14–18]. One can note that these numerical studies are focused on either heart or the blood pump. But simulating hemodynamic inside a patient-specific heart supported with LVAD can help in identifying flow-related irregularities that may raise serious complications like clot formation, blockage, and high shear zones.

However, such efforts are limited in literature [19–22]. Many of these studies were focused on optimal placement of outflow connections to the heart. For instance, Karmonik et al. [19] investigated the effect of orientation of outflow graft on the hemodynamics in ascending aorta. Similarly, Aliseda et al. [20] explored the effect of outflow graft angle on thrombosis risk inside aorta. Recently, Wang et al. [23] analyzed the changes in local hemodynamic parameters inside the aorta after implantation of a short-term LVAD (Impella CP). They have reported the alteration of some important hemodynamic parameters after LVAD implantation in the aorta region.

The existing literature mainly discusses about the investigation of the influence of LVAD on the fluidics inside the aorta only. In some rare attempts where the alteration of fluidics in aorta after LVAD implantation is not the main focus, Ghodrati et al. [24] investigated on the influence of inlet cannula on the risk of thrombus formation. They reported that a higher blood washout to minimize the stagnation probability can be achieved by implanting the inlet cannula at the center of ventricle apex. In the literature, investigation of the influence of LVAD on the entire left heart by considering the inlet cannula and outflow graft altogether has not explored yet. Therefore, the fluidics inside the entire left heart after LVAD implantations require a thorough study. An LVAD (continuous-flow LVAD) implanted heart differs from the normal heart by pumping out the blood in both systolic and diastolic phases. The outflow wave of LVAD's pump comprises the mixture of the non-pulsatile flow of pump and pulsatile flow of heart. Furthermore, in the previous simulation-based study on LVAD pumps, the inlet to pump is assumed to be of the tubular section. However, the ventricular flow pattern may impart a significant effect on the blood pump inlet (as compared to the inlet from an idealized tubular shape) [25]. Therefore, investigations can be made to explore the influence of intraventricular flow on the performance of LVAD.

The present work is targeted to investigate the influence of LVAD pump on the hemodynamics of the native heart. The patient-specific left heart has been simulated with and without LVAD pump to analyze the change in hemodynamic characteristics. Furthermore, emphasis has been given to assess the fluidics inside the LVAD pump in the implanted condition.

2 Methods

2.1 Geometry reconstruction and meshing

To present the realistic cardiac flow, the complex-shaped realistic heart of a healthy human being is desired as a computational domain. Setting the same as criteria, a 3D heart model is generated using the patient-specific medical image datasets of a healthy human being at both diastole and systole phases. The medical datasets were taken from an open-source library (<https://www.osirix-viewer.com>). The CT data of the patient's heart (healthy heart having normal coronary arteries with mild calcifications) were taken in DICOM format. Further details of the patient-related information were not made public for such a retrospective data. Ethics committee approval was not required because all patients provided informed consent for any research involving clinical information. The visuals of the dataset are shown in Fig. 1a, in which various important chambers are identified and marked for both diastolic and systolic phases. An open-source image processing software, 3D Slicer, is employed to segment the images and extract the 3D heart domain in the systolic and diastolic stages. The DICOM datasets contain stacks of 2D tissue image sections which are combined to generate a 3D heart model. The extracted 3D model has been further repaired and cleaned up in the open-source software “Autodesk Meshmixer (<https://www.meshmixer.com>)” and is shown in Fig. 1b and c.

The extraction of mitral and aortic valve from the CT datasets is a bit complex and difficult as they crossed other long-axis images. Owing this difficulty, these valves are externally designed in SolidWorks. These valves are fitted at their usual places in the extracted left heart model. The purpose of the valves in this work is to only allow/prevent blood flow during the respective cardiac phases. The incorporation of a real patient-specific valve may influence the flow pattern near the valves. However, in this work, flow near valves is not considered.

A hemodynamically improved version of the axial LVAD pump proposed in the study of Kannojiya et al. [26] has been considered in this work. The blood pump has been implanted into the LH computationally by using SolidWorks. The inducer and diffuser of the blood pump are fixed to the inner wall of the housing, whereas the impeller is supported on a hydrodynamic bearing with blades that have a clearance of 0.25 mm from the housing. An inflow cannula and outflow graft of 10-mm diameter are also designed to establish a connection between the heart and the blood pump. Blood from LV enters the pump from the inflow cannula and leaves to the ascending aorta via outflow graft. The entire computational domain for diastolic phase has been shown in Fig. 2a.

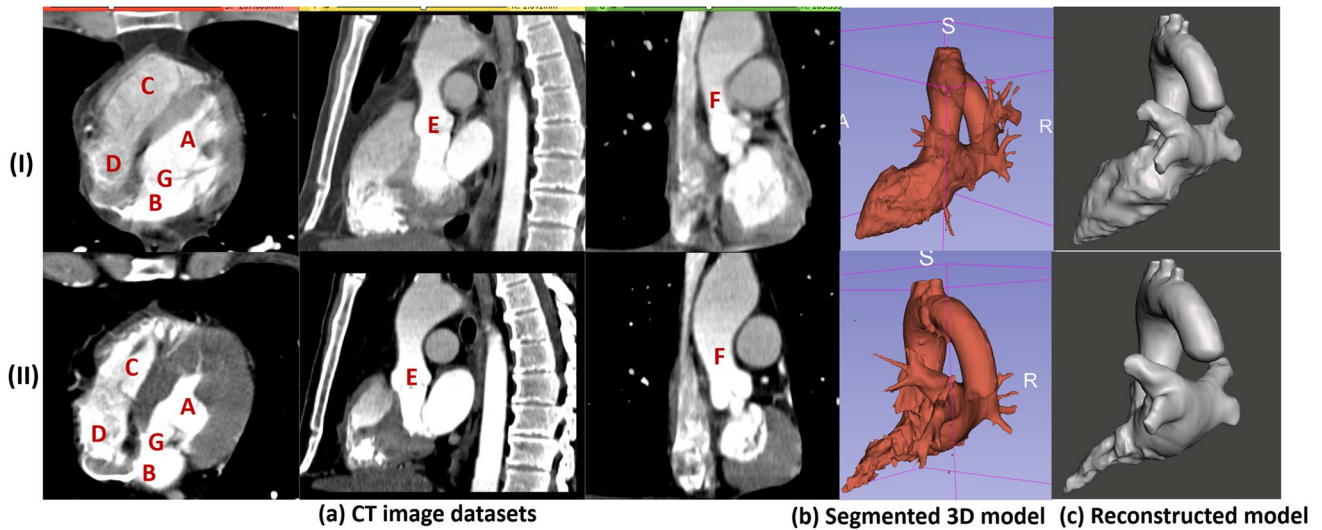
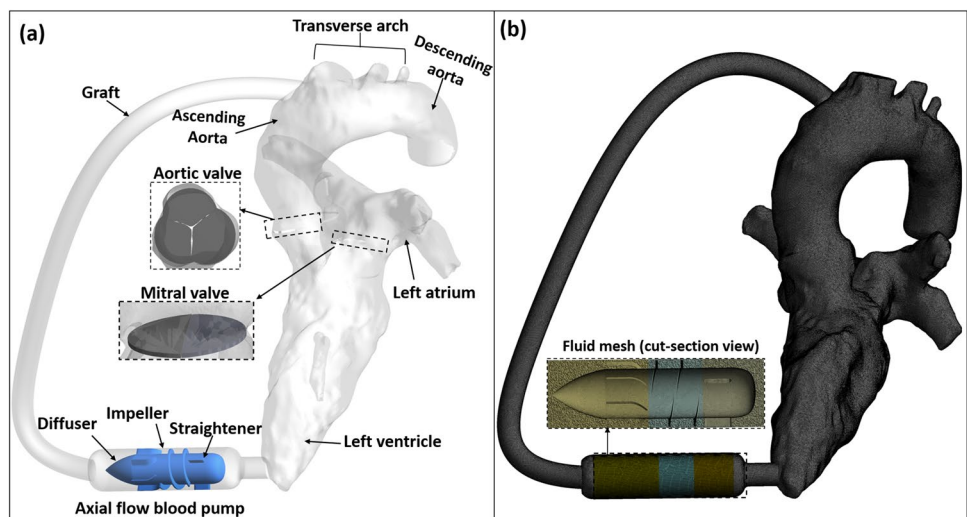


Figure 1 **a** Identification of zone of interest in CT scan dataset; A left ventricle (LV), B left atrium (LA), E aortic valve (AV), F aorta, and G mitral valve (MV) (C and D: right ventricle and atrium; not

included in this study); **b** segmented 3D model of the left heart (LH); and **c** reconstructed LH model after repair for (I) diastolic phase and (II) systolic phase.

Figure 2 **a** Computational domain of LH implanted with axial-flow LVAD blood pump and **b** meshing on the computational domain for diastolic phase.



The computational domain has been meshed into smaller tetrahedral elements by using ANSYS ICEM. A grid independence study has been performed to decide about adequate mesh size within affordable computational cost. Table 1 summarizes the outcomes of grid independence test for both diastolic and systolic phases. It can be observed that for systole, the variation in outcomes saturates when the domain is divided into 4.2×10^7 tetrahedral elements. On the other hand, 3.5×10^7 elements are sufficient to effectively capture the hemodynamic features in diastole. Hence, the number of meshes has been used for discretization of domain in this study. Further refinement in the mesh will not improve the outcomes but yield more computational time. The generated mesh also satisfies the necessary quality conditions

(average skewness ~ 0.23 , Jacobian ratio = 1.18, element quality = 0.96, and aspect ratio ~ 2.80). The representation of mesh generation for diastolic phase has been shown in Fig. 2b.

2.2 Hemolysis estimation

To check the hemocompatibility of blood pump, a hemolysis model was also simulated by solving the transport equation for the entire domain (for LH with LVAD) by using Eulerian approach. The hemolysis model used in this study was suggested by Giersiepen et al. [27], which is also referred as the power-law relation. This model represents the amount of hemolysis as a power-law function of shear stress magnitude

Table 1 Fluidic outcomes of the heart implanted with LVAD at different grid sizes

Number of elements	At descending aorta			
	End diastole		End systole	
	Flow rate (L/min)	WSS (Pa)	Flow rate (L/min)	WSS (Pa)
7.8×10^6	6.35	13.41	4.87	11.87
1.2×10^7	6.57	13.52	5.02	11.96
2.8×10^7	6.68	13.58	5.09	12.02
3.5×10^7	6.75	13.63	5.14	12.07
4.2×10^7	6.80	13.67	5.14	12.09
4.4×10^7	6.81	13.69	5.14	12.09

(τ) and exposure time (t_{exp}), integrated along the path from inlet to the concerned cell. The equation of this model to calculate hemolysis index (HI) can be written as follows:

$$HI(\%) = \frac{\Delta HB}{HB} \% = C t_{exp}^a \times \tau^b \quad (1)$$

The values of constants mentioned in the above equation are taken from the study of Taskin et al. [28] ($C = 1.21 \times 10^{-5}$, $a = 0.747$, and $b = 2.004$). They observed only a 5% variation in the value of hemolysis index calculated by experimental and numerical methods. Furthermore, the value HI has been utilized in the estimation of the normalized index of hemolysis (NIH), which can be expressed as follows:

$$NIH(g \text{ per } 100 \text{ L of blood}) = 100 \times HI \times (1 - H_{ct}) \times k \quad (2)$$

Here, H_{ct} is the hematocrit (considered as 45% in this work) and k is the hemoglobin content of the blood (150 g L^{-1} for a healthy human) [29].

Further details of the hemolysis modeling can be found in these studies [16, 26].

2.3 Computational setup

The simulation framework is setup by using commercial finite volume CFD code ANSYS-FLUENT 16.0. A pressure-based solver is employed to solve the

hemodynamics, while the pressure–velocity coupling is achieved using SIMPLEC scheme. The governing equation (Navier–Stokes) is discretized at each control volume by a second-order upwind scheme. For simplification of study, the heart wall is assumed as rigid, and no-slip condition is assigned to it. In this study, the LH wall (LA + LV) is static throughout the simulation. The prime objective of including static left heart is not to mimic the cardiac deformation that requires a complex numerical framework. Instead, it is included to generate complex cardiac flow.

The patient's heart rate is assumed to be 75 beats per minute; one cycle lasts for 800 ms. The simulation is performed for three cardiac cycles. The simulation results have been considered after three cardiac cycles to circumvent the initial effects. It should be noted that during the LVAD support, the aortic valve opens once in every five cardiac cycles [30, 31]. In this study, the cardiac cycle at which the aortic valve is open is considered. The details of the boundary conditions are summarized in Table 2.

The blood pump's inlet and outlet have been assigned an interface condition to allow the blood flow passage through it. The pump's straightener and diffuser were kept stationary, whereas rotating frames are assigned to the impeller. The impeller is linked with the adjacent blood layer by using a suitable interface. The timesteps for the analysis are selected as 0.04 ms to yield less than 2° rotation of the pump at operating speed (8000 rpm).

Table 2 Boundary conditions for simulation setup

Boundary conditions	Type			
	Normal heart		Heart with LVAD support	
	Systole	Diastole	Systole	Diastole
Pulmonary vein (Inlet)	Mass flow profile [32]	Wall: no slip	Mass flow profile [32]	Wall: no slip
Aorta (Outlet)	Velocity profile [33]		Pressure: 100 mm Hg [34]	
Mitral valve	Wall: no slip	Interface	Wall: no slip	Interface
Aortic valve	Interface	Wall: no slip	Interface	Wall: no slip

Blood is a shear-thinning fluid, and its viscosity decreases with increase of shear rate. The rheology of blood depends on many parameters such as shear rate, domain diameter, temperature, hematocrit (volume percentage of red blood cell in blood), etc. It is suggested in many studies that blood behaves as Newtonian fluid at shear rates higher than 100 s^{-1} . However, it is not necessary that every region of the heart is exposed to a shear rate higher than the mentioned limit during the entire cardiac cycle. A constant blood viscosity assumption might not be sufficient in such a case, which was also reported by Doost et al. [35]. Therefore, to precisely capture the hemodynamics through the heart, the blood viscosity is modeled by considering Carreau model [36]. This model can effectively characterize the rheology of both the shear thinning and shear thickening fluids. It is typically a combination of Newtonian and Power-law model. This model overcomes the shortcoming of the Power-law model and is effective at both high and low shear rates [37]. The governing equation for viscosity by this model can be expressed as follows:

$$\mu = \mu_{\infty} + (\mu_0 - \mu_{\infty}) \left[1 + (\lambda \dot{\gamma})^2 \right]^{\frac{n-1}{2}} \quad (3)$$

The model parameters are taken from the study of Cho and Kensey [38] in which they have fitted the Eq. (1) with their experimental data. The high-shear μ_{∞} and low-shear viscosity (μ_0) are taken as 0.00345 Pa.s and 0.056 Pa.s, respectively, whereas the value of time constant (λ) and power-law index (n) for the simulation has been selected as 3.313 s and 0.3568, respectively [39, 40].

The k- ϵ turbulence model along with enhanced wall treatment approach has been employed to solve the flow turbulence. This model is computationally inexpensive to other widely used models such as k- ω and SST models. However, it has certain shortcomings in capturing the near-wall phenomenon. The use of enhanced wall treatment method in the k- ϵ facilitates the resolution of near wall flow; moreover, this approach is also effective to capture both high- and low-energy flows. Many researchers [41, 42] have adopted k- ϵ model in blood flow modeling inside the human heart. Furthermore, Jahanzamin et al. [13] reported that k- ϵ model provides more closer prediction to the experimental findings. Even in our previous study for optimization of pump design [26], we have tested several turbulence models and found k- ϵ model to be most accurate. Based on this literature support, though for different geometries, in present study, we have adopted k- ϵ turbulence model. The computations are performed in series by using a Dell server (Power-Edge R730) with Intel(R) Xeon(R) processor E5-2600 v4 (128 GB RAM).

2.4 Verification of numerical framework

To verify the accuracy of the numerical simulation, the results of the present study are compared with the findings of Dahl et al. [32]. They have simulated hemodynamics inside a left atrium. In particular, the influence of pulmonary venous location on the fluidics inside the left atrium was discussed in their study. They have utilized different flow rates at the pulmonary inlet veins as obtained from the mapped MR scan datasets. A numerical simulation has been carried out by imposing similar conditions (as mentioned in the subgraph of Fig. 3) on our computational domain (diastolic phase of healthy heart without LVAD). Figure 3a shows a satisfactory comparison of the maximum transmitral velocity as obtained in the present study and in the work of Dahl et al. [32]. Furthermore, nearly similar velocity profile has been also noticed at the mitral plane, as shown in Fig. 3b.

In a similar attempt, the simulation framework is also validated with the experimental findings of Sang and Zhou [43] by considering only blood pump as the computational domain. Sang and Zhou [43] have analyzed the performance of axial-flow LVAD by employing xanthan gum as the working fluid using the experimental and numerical technique. The details of the validation results can be found in our earlier work [26].

3 Results and discussion

The numerical analysis has been performed for two cases: simulation of the left heart without any LVAD support and simulation of the left heart supported with axial LVAD. The outcomes of both the cases have been summarized for the two cardiac phases: systole and diastole phase. Each cardiac phase is divided into three major intervals: early (beginning), peak (middle), and end depending on the time interval. The results at different intervals of both the phases at distinct locations are discussed in the subsequent sections.

3.1 Systole phase

3.1.1 Flow inside aorta

Aorta is the largest artery responsible for transmitting blood flow from the heart to different organs. A major change in hemodynamics after implantation of LVAD is observed inside the aorta. To understand this change, initially, velocity vectors are plotted at different stages of systole phase on the middle sectional plane of the aorta for the native heart case (without LVAD support), as shown in Fig. 4A. The timepoints of different intervals of systole phase were also marked in Fig. 4A; similar timepoints have been considered in evaluation of further results at systole phase. The aortic

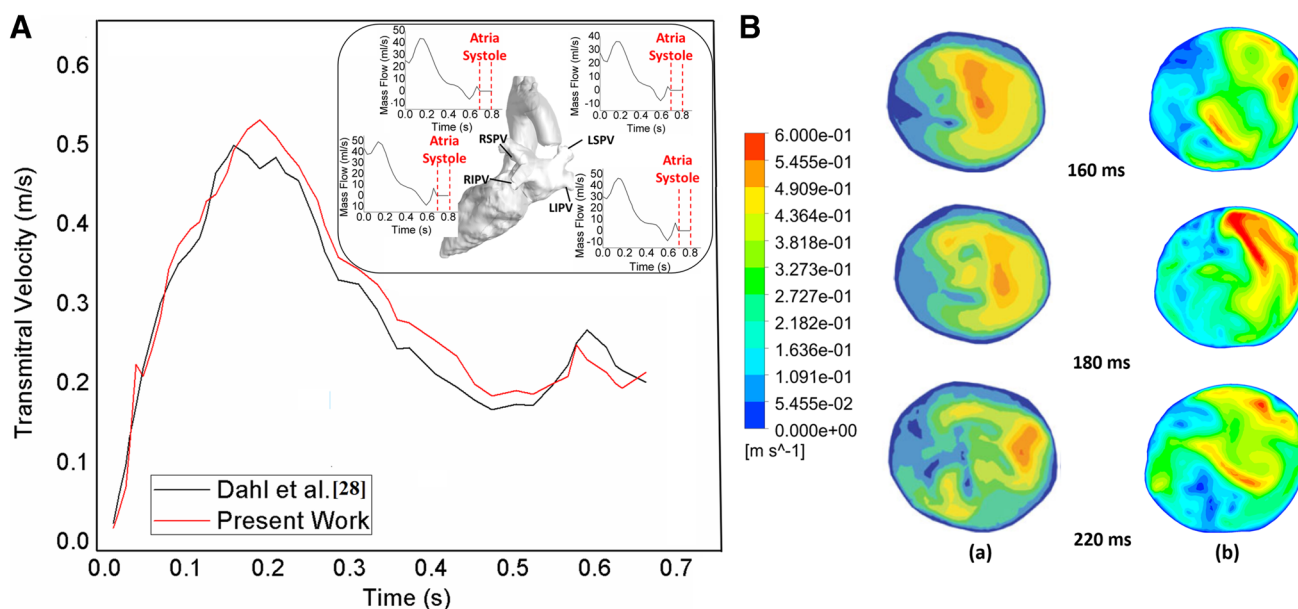


Fig. 3 **A** Comparison of fluidic outcomes with the numerical study of Dahl et al. [32]; imposed boundary conditions are shown in inset. **B** Contours of velocity at mitral plane for a Dahl et al. [32] and b present work at different instances of diastolic phase

section experienced very random and mixed flow during the end stage of the systolic phase. However, the flow path is noticed to be well organized during the peak systole phase. During the entire systole, the flow is well distributed and unidirectional inside the aorta. However, similar is not the case after LVAD implantation.

Figure 4B shows the velocity vectors at the aorta after the implantation of axial LVAD. During the early systole stage, the blood stream coming from the pump through the graft bifurcates into two streams. A major part of the flow advances towards the descending aorta, while a slight flow is also noticed towards the ascending aorta. However, as the systole phase advances, a mixing of blood streams coming from the pump through outflow graft and left ventricle through aortic root is noticed at the ascending aorta region. It should be noted that the heart's natural outflow is observed to very low as compared to the pump outflow. At the ascending aorta, a low flow region away from the wall is formed due to the mixing of low flow from native heart and the pump outflow. However, significant flow is still observed near the wall regions. On the other hand, a well-distributed but highly mixed blood wave advances from the descending aorta to different body organs. At the end of the systole phase, this low flow region's intensity at the ascending aorta is further increased as the major part of the flow is only contributed by the blood pump. Therefore, after the LVAD implantation, the flow profiles at the aorta are majorly changed.

To further compare the change in hemodynamics of LH after LVAD implantation, velocity contours are plotted at

different sections (planes A to G) of the aorta during peak systole for both the cases (LH with and without LVAD), as shown in Fig. 5. Here, planes A to C represents the ascending aorta, D and E signify the aortic arch region, and descending aorta zone is presented by planes F and G. It can be observed that for native heart, variation in velocity profile at different sections of aorta is not much significant as compared to the LVAD implanted heart. The velocity profile appeared to be well distributed at planes A and B of Fig. 5a. However, a low-velocity spot is noticed at the upper section of plane C due to increase in the flow area. As the flow further advances, it gains more momentum due to reduction in flow area from arch region to descending aorta (planes D to G). In these regions, not much change in the flow profile is noticed apart from the flow magnitude. The highest magnitude of velocity is noticed at plane G (2.6 m/s at 11.2% of total plane area) as the flow domain gets narrower with the distance.

The velocity profile of heart supported with LVAD differs hugely from the native heart over the entire aortic region, as represented in Fig. 5b. As most of the flow is contributed by blood pump, some low-velocity region (nearly 0.09 m/s at 9.3% of total plane area) is noticed in the upper section of ascending aortic root (plane B). On the other hand, at plane C, a sudden variation in flow profile is noticed as some of the incoming flow streams from the graft also enters up to this region (plane C) and gets mixed with the flow from LH. At plane C, high velocity of 0.76 m/s is at 0.27% of total plane area at the bottom of the plane, whereas the upper wall region experiences low flow velocity of 0.09 m/s.

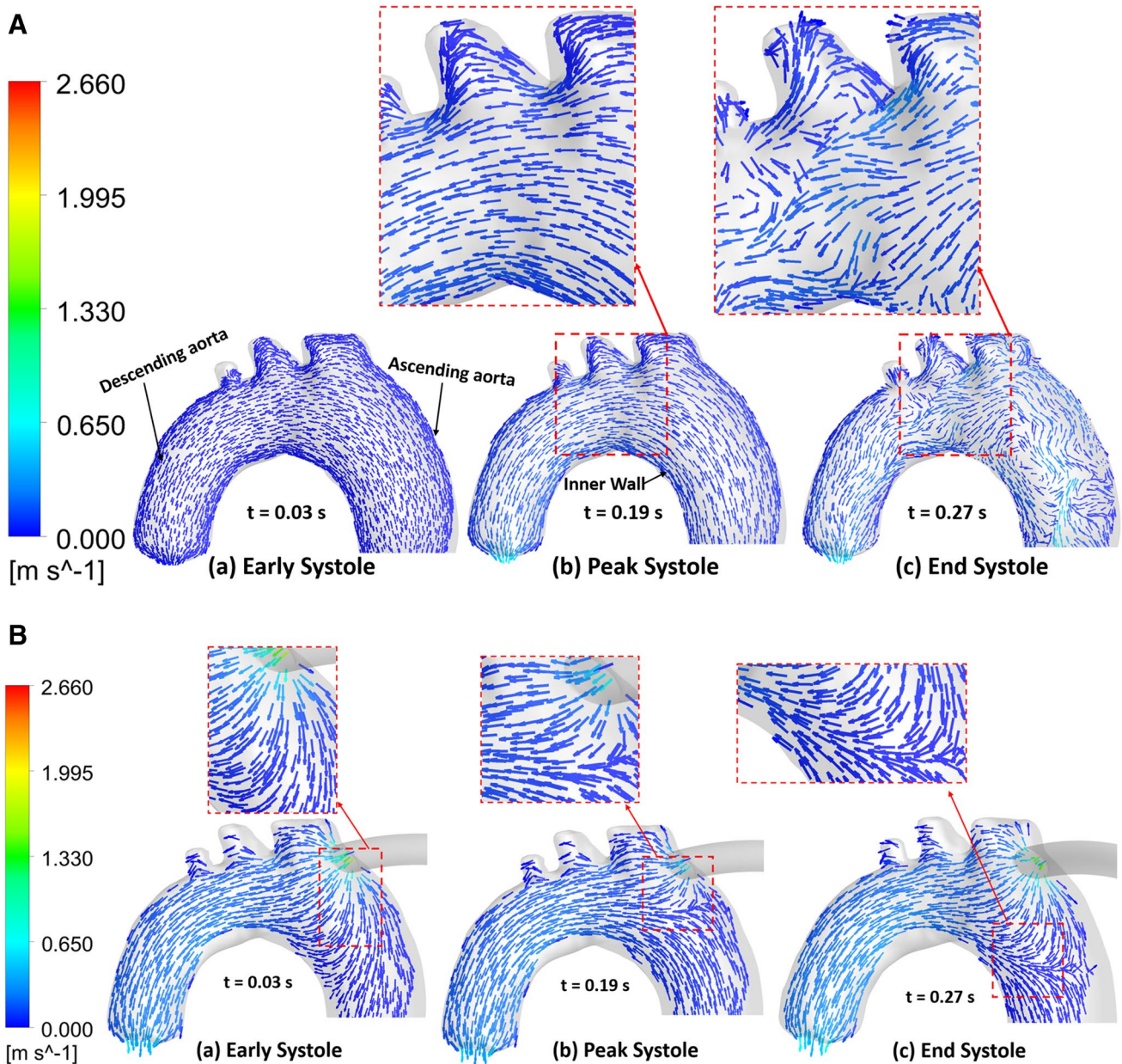


Fig. 4 **A** Velocity vectors at the central plane of aorta for native heart (without LVAD support), showing high flow mixing during early and end systole. **B** Velocity vectors at the central plane of aorta after implantation of axial flow LVAD to the heart

Furthermore, at plane D, due to entry of blood from pump, a high magnitude of the velocity is noticed at the aortic arch region. This flow further advances inside the aorta and gets well distributed to the complete domain circumferentially at the descending aorta region (shown in planes E, F, and G). A high-velocity region (nearly 2.57 m/s velocity at 4.57% of the total plane area) is also observed at plane G due to the lower cross-sectional area there, and also, the flow is now supported by gravity. Hence, the profiles demonstrate a significant change in the hemodynamics inside the aorta due to the implantation of axial-flow LVAD to the LH.

The blood pump can significantly alter the cardiac output at a particular rotational speed (8000 rpm is the operating speed in this study). The average outflow rates are measured at different stages of the systolic phase to analyze the change in cardiac output, as shown in Fig. 6. At the descending aorta, the blood flow rate for the normal heart (without LVAD) is much higher (nearly 9.4 L/min) at the peak of systole phase than the early and end-systolic phases. The flow rate profile for the normal heart at the descending aorta is in line with the flow rate profile measured by the MRI datasets by Bensalah et al. [44]. On the other hand, flow rate of 6.15

Fig. 5 Velocity contours over the aorta for the A native heart and the B heart supported with axial flow LVAD

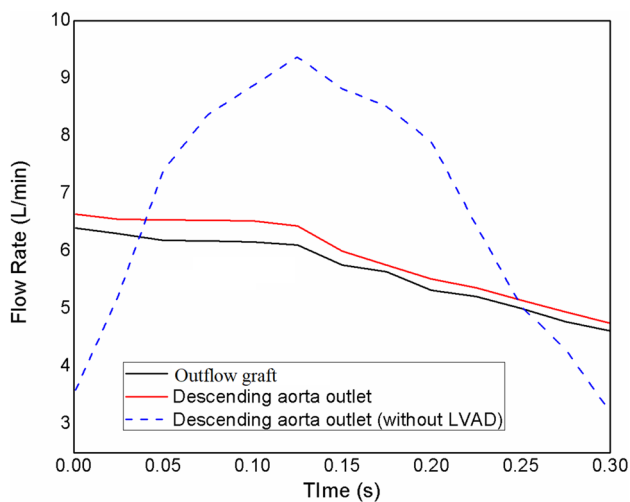
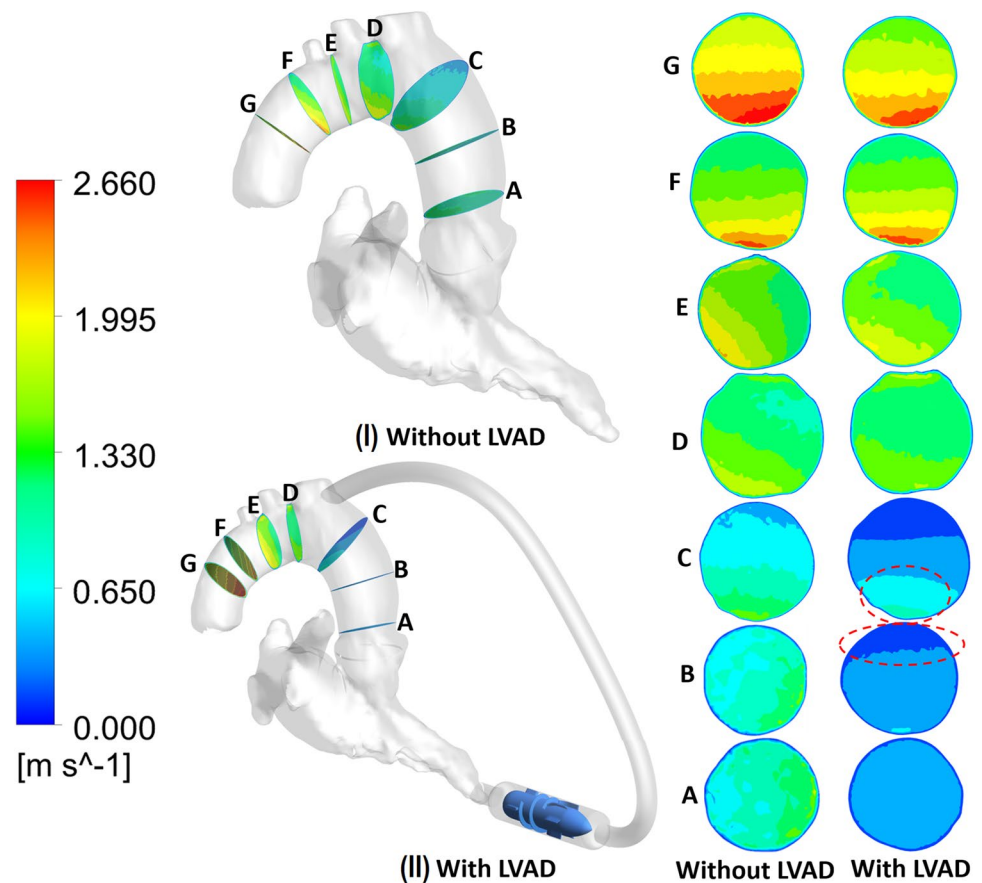


Fig. 6 Flow rate distribution at the outflow graft and descending aorta during systole

L/min is noticed at the early systole for heart supported with LVAD. At the end of systolic phase, a sharp reduction in the outflow is noticed as the ventricle is left with lesser blood.

It has also been noticed that the implantation of blood pump alters the ventricle unloading pattern. Figure 7 shows

contours along a section plane to show the velocity distribution at ventricle and some regions of aorta and atrium. In normal circumstances (without LVAD), the ventricle ejects out through the aorta only (Fig. 7b). The average velocity at the aortic plane during the peak systole was noticed as 1.31 m/s. However, after LVAD implantation, very low flow is noticed at the aortic root during the early systole. Furthermore, as the systolic phase advances, the major fluid transfer occurs from the ventricle apex to the aorta through the blood pump and graft. The average velocity at the aortic plane and the plane at ventricular apex during the peak systole was noticed as 0.19 m/s and 1.27 m/s. The change in the outflow location during systole does not affect the heart's ultimate purpose, i.e., providing the adequate cardiac output to sustain the life. Though acute unloading of left ventricle may affect the right ventricle's contractility [45], but as per Fig. 6, no excessive enhancement in cardiac output is noticed. In the subsequent section, the change in hemodynamics inside blood pump is discussed.

3.1.2 Flow inside blood pump

After the aorta, a significant change in hemodynamics is noticed inside the blood pump. Figure 8 shows the velocity vectors at the central plane of blood pump during different

Fig. 7 Velocity contours plotted along a sectional plane during different stages of systole

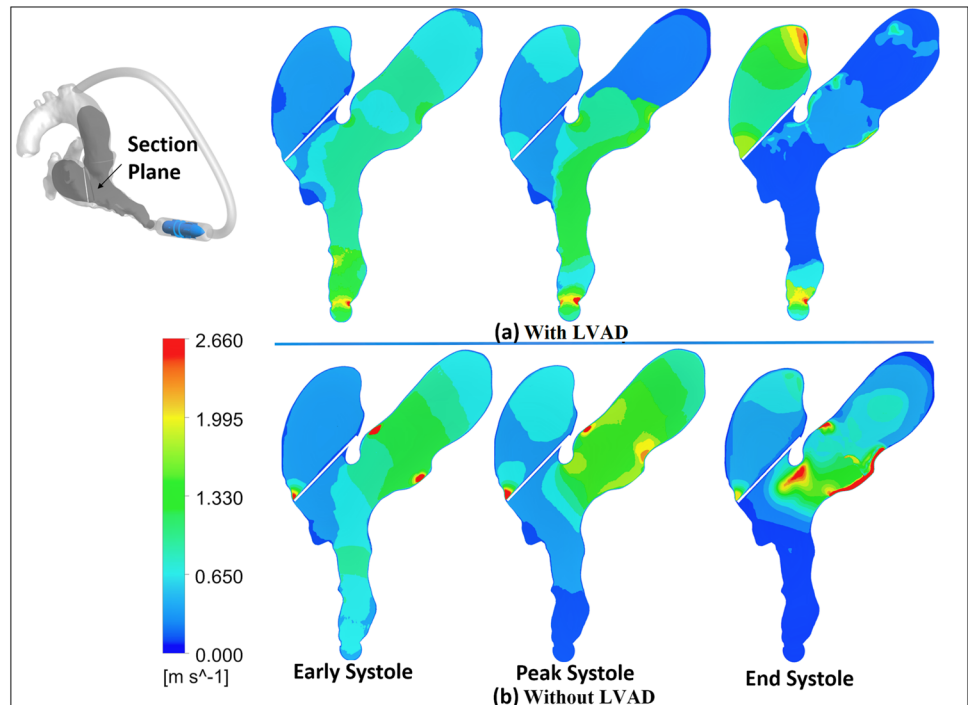
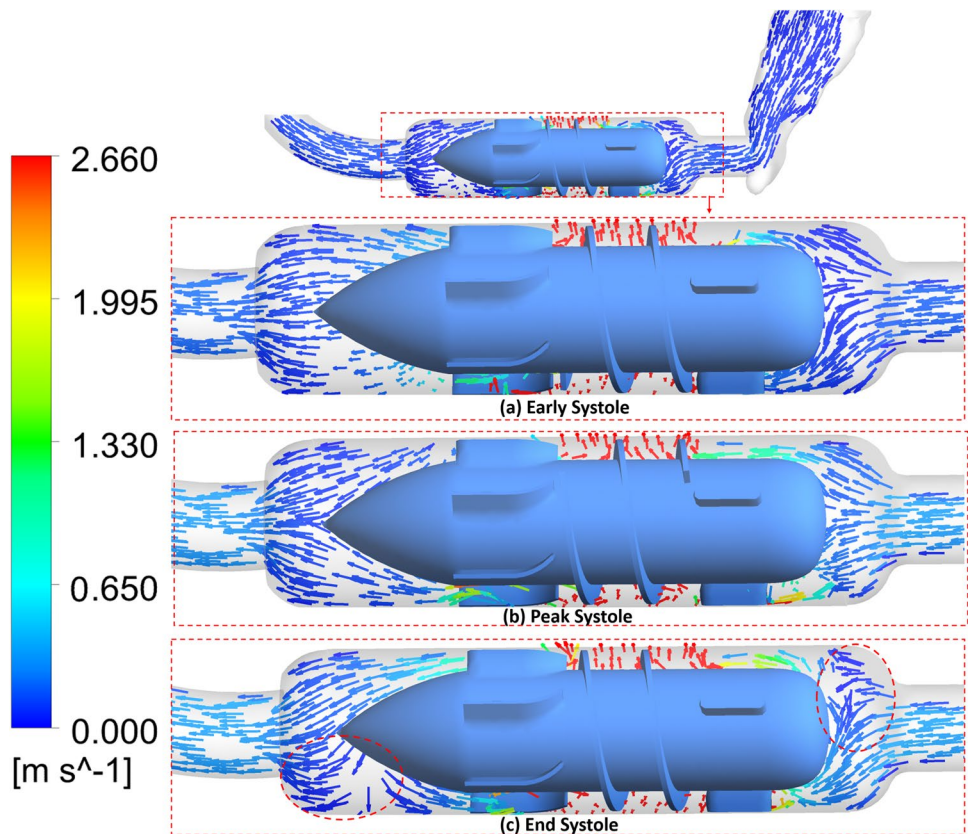


Fig. 8 Fluidics inside the axial flow blood pump during ventricular systole



stages of ventricular systole. The impeller’s rotating action drives the blood from the left ventricle to the pump through the inflow cannula at the early systole (Fig. 8a). It can be

seen that the flow distribution is uniform inside the pump at the starting and peak of the systole phase (Fig. 8 a and b)). Eventually, the flow inlet to the pump from the ventricle is

reduced at the end of systole, but the heart is not completely emptied. It should be noted that the mitral valve is closed during this phase. The majority of the flow to the pump is coming from the downward section of the inflow cannula which may be due to the uneven flow distribution at the ventricular apex. Simultaneously, a low-velocity region can also be noticed in the upper section at the inflow cannula. This shift of flow velocity in the cannula results in forming a low-pressure area in the upper section of the pump near the straightener (marked in Fig. 8c). Hence, a flow reversal is noticed at the inlet of pump due to the development of a pressure gradient inside at the end of systolic phase. However, the pump is capable of delivering sufficient flow rate during the entire systolic phase. The average pump output (measured at the cannula-aorta junction) at end systole is approximately 4.57 L/min, whereas it is 5.14 L/min for the entire systolic phase.

The flow profile inside the blood pump varies over the different instants of the systolic phase as the flow output of ventricle is not uniform at every instant of systole. Generally, the LVAD pumps are widely simulated by assuming a tubular flow inlet to the pump. We believe that the ventricular flow pattern can influence the flow characteristics of the blood pump. A simulation case of blood pump without any load (without inflow from heart) has been executed to investigate this. The measured average inflow and pressure outlet (from the on-load condition results) are assigned as the boundary condition to the pump. The velocity field after achieving the convergence is shown in Fig. 9. As depicted in the figure, the velocity profile inside the blood pump is observed to follow a uniform path. The pump's flow looks smoother and more stable compared to the more realistic case (LVAD implanted to the heart or on-load condition). This variation in flow field in the general simulation approach may also lead to discrepancies in the actual characteristics curve, generated shear, and pump efficiency. As simulation strategies are continuously developing to enhance the prediction accuracy; therefore, the inclusion of the left

heart or left ventricle in the simulation of LVAD pumps can open a future research area regarding the same.

3.1.3 Effect on shear generation

The implantation of LVAD not only alters the hemodynamics of heart but also elevates the generated shear stress. To observe this change, contours of wall shear stress (WSS) are plotted at different systolic phase stages for both cases (LH without LVAD support and LH with LVAD support) and shown in Fig. 10. The WSS on the LH without LVAD support is observed to be significantly less than its counterpart. The aortic sinus region experienced the highest wall shear stress during the entire systolic phase. However, some high shear spots were also noticed at the mitral valve annulus during the early systole and at descending aorta during the end of systolic phase (Fig. 10a).

After implantaion of LVAD to the LH, the distribution of WSS changes significantly. The highest shear stress is noticed on the blood pump. Considerable high shear spots were also observed at the cannula, particularly at the tube's bending sections. However, high shear zones at heart are very less and observed only at the mitral valve annular during the early systole (Fig. 10b). As the systole phase further progresses, high shear stress on the heart is almost negligible as compared to the blood pump. At the end of systole phase, average WSS of 97 Pa was noticed at 6.21% volume of the heart supported with LVAD, majorly located at the LVAD pump (nearly at 27% volume of LVAD pump), whereas around 2.73 Pa WSS was observed at 1.79% volume of the heart (without LVAD). In particular, for aorta region, the average WSS for the normal heart was observed to 2.3 Pa. Similar range of WSS at the aorta for large number of patient's population ($n=224$) is also reported by Callaghan and Grieve [46]. On the other hand, for the LVAD implanted heart, the average WSS elevates to 16.84 Pa. The magnitude of WSS is in agreement with the WSS observed at the aorta in the study of Karmonik et al. [19]. It should

Fig. 9 Velocity vectors inside the blood pump at off-load condition (without implantation to the heart)

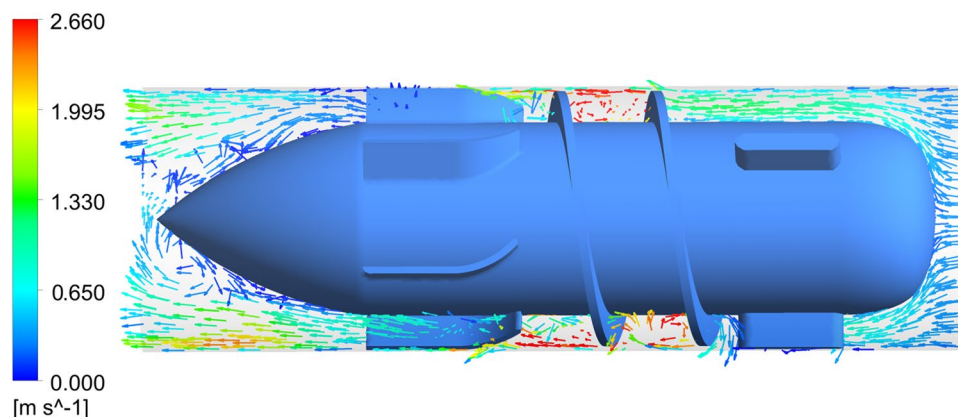
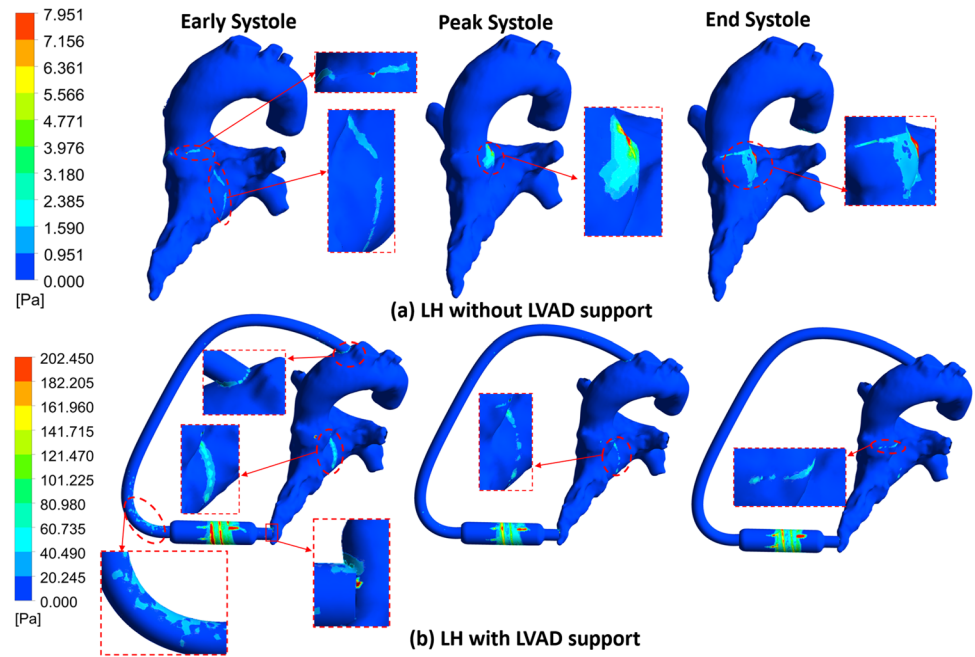


Fig. 10 Shear generation on the wall of the **a** left heart and the **b** left heart supported with axial LVAD during systole



be noted that higher shear stress can damage the blood cells and may lead to hemolysis.

The normalized index of hemolysis (NIH) calculated at the outlet of blood pump, graft outlet, and ascending aorta was found to be 0.0091 g/100 L, 0.0069 g/100 L, and 0.0048 g/100L, respectively, Though, the implanted LVAD significantly elevates the shear stress inside the heart. However, the index of hemolysis is well within the permissible limit (0.01 g/100 L for long-term implantable device [47]).

Furthermore, investigations on the change in heart’s hemodynamics due to LVAD implantation are also carried out for the diastolic phase, as discussed in the next section.

3.2 Diastole phase

3.2.1 Flow inside the aorta

After implantation of continuous-flow LVAD, the aorta transfers blood flow to other organs at both the systole and diastole phases, during the diastolic phase, as the aortic valve is closed; therefore, no blood flow is noticed from the native heart. However, the pump is continuously delivering the blood to the aorta. To understand the fluidics during the diastole phase, velocity vectors (scaled to the same velocity magnitude as observed during systole phase) are plotted at the central plane of the aorta, as shown in Fig. 11. It can be seen from the figure that the bloodstreams entering the aorta from the cannula get bisected into two streams (Fig. 11a). The flow streams are now moving toward the descending aorta and also towards the aortic root, simultaneously. However, as the

aortic valve is closed during the diastole phase, the blood-streams are restricted to the aortic root only. As the diastolic phase progresses further, flow reversal in the second bloodstream (towards the aortic root) is noticed (Fig. 11b). The flow vectors started to change their direction from being towards the aortic root to the ascending aorta due to the development of an adverse pressure gradient. This phenomenon is further accelerating at the end of the diastolic phase, and mixing of blood streams is noticed, as shown in Fig. 11c. The blood near the aortic root probably gets mixed with the natural flow from the ventricle and carried forward during the next systolic phase (as the aortic valve opens during the systole). Hence, a major change in the hemodynamics of LH is noticed at both systolic and diastolic phase.

The pump is capable of delivering an adequate flow rate (required as per the human physiology) during the diastolic phase. The measured average flow rate at the descending aorta is observed to be 4.87 L/min. The variation in flow rates at different intervals of the diastolic phase is represented in Fig. 12. At the early diastole, lesser outflow is noticed due to the lower availability of the blood at the ventricle. However, as the diastole further advances, the ventricle starts to fill with blood, and the blood pump’s outflow increases nearly by 50%. The discharge gets stabilized, and an almost constant flow rate is noticed during peak and end systole. Significant enhancement in the cardiac output during diastolic phase is noticed after LVAD implantation. However, this enhancement comes at the cost of higher shear generation, as discussed in the further subsection.

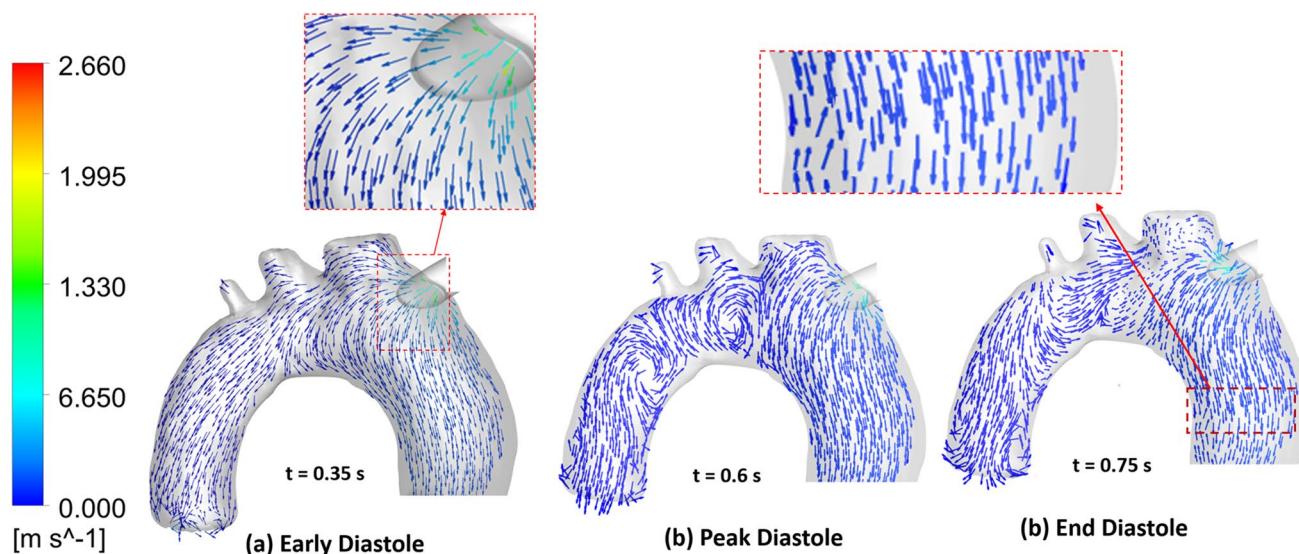


Fig. 11 Velocity vectors at the central plane of aorta, showing flow bisection during diastole

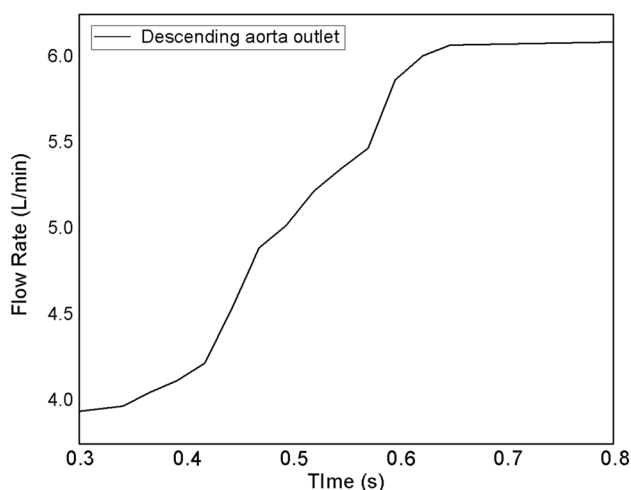


Fig. 12 Flow rate distribution at the blood pump outlet and descending aorta during diastole

3.2.2 Effect on shear generation

The influence of LVAD implantation on the shear stress generation is also investigated for the diastolic phase. Figure 13 shows the contours of WSS for LH with and without LVAD support plotted at different instants of diastolic phase. Again, a significant change in the magnitude of shear stress and its generation pattern is observed due to LVAD implantation. For a normal heart (without LVAD), it is noticed that high shear spots are only observed at very few locations of the heart and are majorly located at the mitral valve annulus and aortic sinus (Fig. 13a). The average WSS on the normal heart was observed as 1.71 Pa and located at only 1.22% volume of the heart. The other

regions of heart wall have experienced comparatively much lesser shear.

On the other hand, the maximum WSS for the LVAD-supported heart is mainly concentrated on the blood pump. However, significant shear is also noticed on the cannula; regions like ventricle-cannula junction and the bending curvature are the most affected zones (Fig. 13b). Some high shear zones are also noticed near the ascending and arch region of the aorta during the peak diastole. The same is eventually reduced at the end of the diastolic phase and is observed to be spread over lesser regions. The possible reason for such high shear in the all the mentioned locations is the sudden change in the blood flow domain. For the entire domain, the average WSS was noticed as 78.43 Pa and was spread over 1.53% volume of the entire domain.

The quantitative distribution of average WSS on ventricle and aorta (ascending + arch + descending) of the left heart is represented in Fig. 14. It can be noticed that for the heart without LVAD, ventricle experiences more WSS than the aorta. Due to the no-flow condition at the aorta during diastolic phase, the WSS at the aorta was observed to be negligible. However, when the heart is supported with LVAD, the WSS generation on both the ventricle and aorta elevates to significantly higher values. For instance, at the ventricle, nearly 18.1 times more WSS is noticed after LVAD implantation. The majority of the high shear zone is focussed only on the ventricle apex. On the other hand, at the aorta, WSS increases drastically from negligible (in case of without LVAD support) to approximately 11.9 Pa (average is taken for entire diastolic phase) after the LVAD implantation. The NIH calculated at the outlet of blood pump, graft outlet, and ascending

Fig. 13 Shear generation on the wall of the **a** left heart and the **b** left heart supported with axial LVAD during diastole

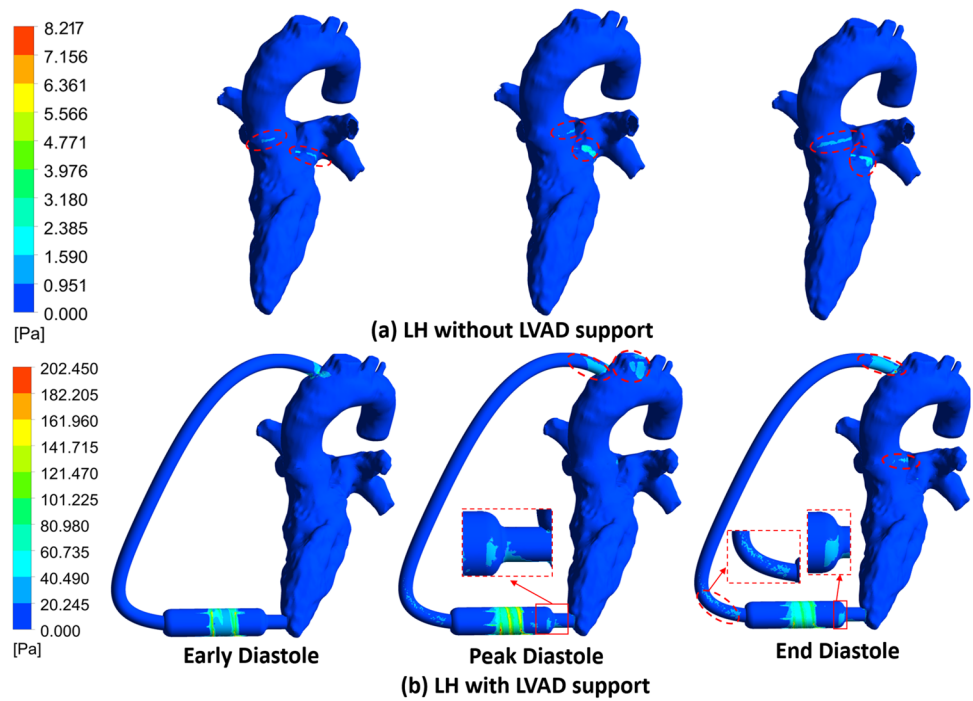
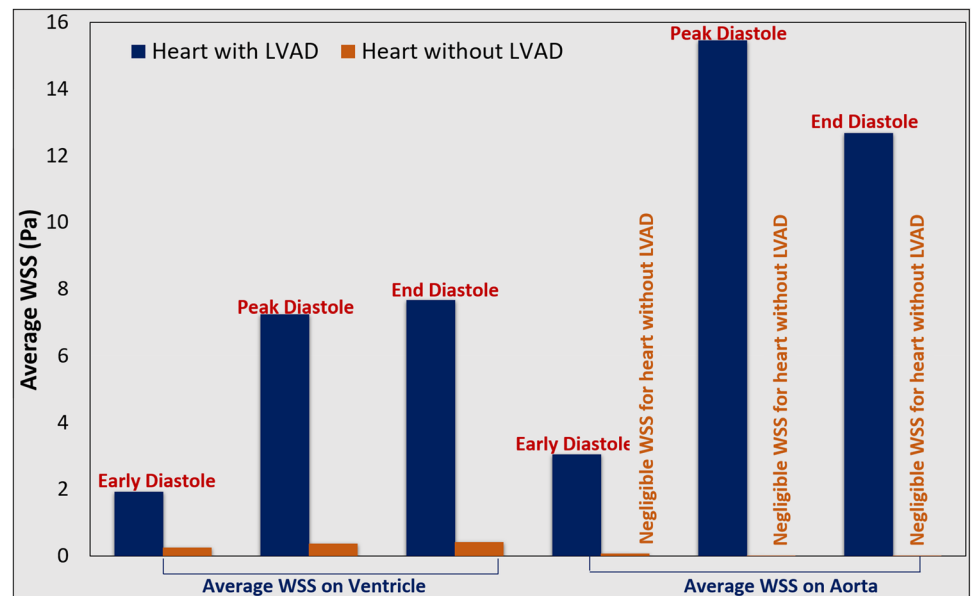


Fig. 14 Average WSS on ventricle and aorta during different stages of ventricular diastole

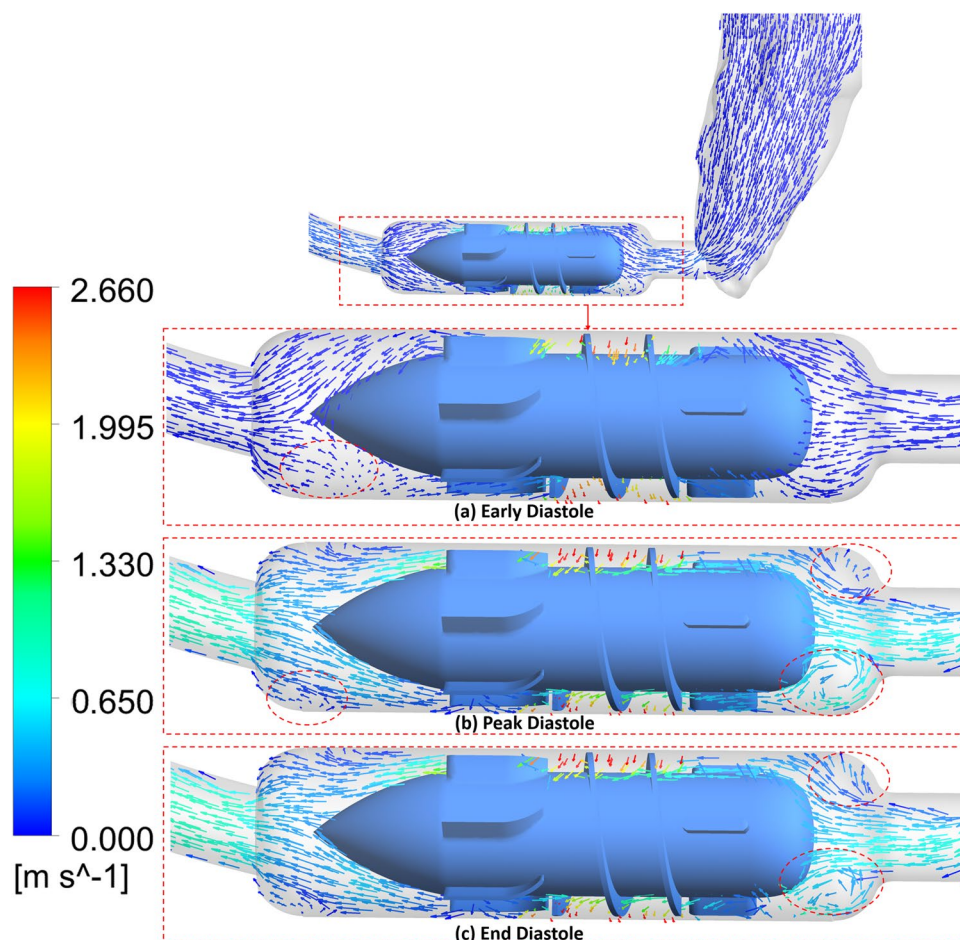


aorta were found to be 0.0091 g/100 L, 0.0077 g/100 L, and 0.0049 g/100L, respectively. The obtained NIH value is lesser than the permissible limit of NIH suggested by the US food and drug administration (0.01 g/100 L) [45]. Therefore, despite the elevated shear generation, the axial-flow LVAD seems to be safe from hemolysis perspective. Furthermore, in the subsequent section, the fluidic characteristics inside the blood pump are also investigated during the diastolic phase.

3.2.3 Flow inside blood pump

Continuous-flow blood pump delivers the cardiac output even in the diastolic phase. In this phase, as the mitral valve opens, the ventricle starts to fill with this blood coming from the atrium. The implanted pump works continuously and delivering the fresh incoming blood from the ventricle to the aorta. Figure 15 shows the hemodynamics features inside the blood pump during three different stages of diastole. Again, the blood pump is subjected to variable inflow

Fig. 15 Fluidics inside the axial flow blood pump during ventricular diastole



conditions, as lower flow input is observed at the early diastolic phase (Fig. 15a). At the beginning of the diastolic phase, blood enters from the ventricle with lesser volume flow rate, resulting in the mixing of bloodstreams at the diffuser (as represented by the highlighted area in Fig. 15a). As the diastole advances, the pump drives the blood with higher flow rate, due to which lesser recirculation is noticed in the diffuser region (Fig. 15b). However, due to the impact of bloodstreams with higher velocity (from the ventricle) on the straightener, a comparatively low-pressure zone is formed at the inlet's upper and lower corner. The low-pressure zone results in the formation of small recirculation zones during the peak systole. During the end of systole, the flow magnitude is further increased (Fig. 15c). Furthermore, nearly the same flow pattern is noticed at the pump inlet. However, flow at the diffuser is appeared to be more stabilized.

4 Study limitations and future directions

Due to the involvement of a complex computational domain, it is really challenging to model the cardiac motion of heart walls. Therefore, the motion of heart wall is not considered

at the intermediate stage of diastole and systole. In fact, two different computational domains have been used generated at the end of diastole and systole. Similarly, the motion of aortic wall is only considered at the end of diastolic and systolic phase, whereas it is assumed as a rigid wall during the intermediate instants of the cardiac phases. The elasticity of aortic wall at the intermediate may impart a noticeable influence on the hemodynamics. However, the inclusion of the inflated and relaxed position of the aortic wall in the study will also provide sufficient details of the complex fluidics inside it.

Several previous studies [41, 48, 49] have assumed rigid wall for their computational domain due to the complexities involved in numerical simulations. It should be noted that fixed-wall simulations may oversimplify inflow-outflow boundary conditions and neglect atrial-ventricular interactions. The atrial-ventricular shape at the intermediate phases of the cardiac cycle may also influence the flow profile in the blood pump. Furthermore, there are chances of difference in the value of instantaneous quantities (flow velocity, WSS) as compared to moving wall simulations [50]. However, there is not much change in time-averaged quantities for both the simulations [51].

Furthermore, the inclusion of realistic heart valves (effects of the trabeculae and papillary muscles) can influence the adjacent flow pattern. However, flow near the valve is not the major consideration of this work as the main purpose of this work is to analyze the influence of LVAD on the change in hemodynamic characteristics of the heart. The valves (mitral and aortic) are designed manually using a CAD software due to the lesser available details of valves in the CT datasets. Valves are mainly employed to allow/prevent the blood flow at the respective cardiac phases. In practical condition, the mechanism of opening of valves is driven by the pressure exerted by the fluid that pass through the valve orifices. On the contrary, in this study, a sudden opening and closing condition have been created by changing the boundary conditions. Though, inclusion of realistic segmented heart valves and their actual dynamics can yield a more accurate numerical framework to simulate the fluidics inside the heart and enhance the prediction accuracy. The lack of experimental data limits the validation of the results. Last of all, this study is based on a single subject under rest conditions; the effect of different subject populations and exercise conditions is not considered. In the present study, location of inflow and outflow connections has not been varied. The same can be optimized through parametric studies as an extension of this work. Hence, a numerical investigation of the left heart with LVAD implanted condition can be planned by overcoming all the limitations as mentioned above.

5 Conclusion

In this work, a patient-specific simulation of a human left heart supported with axial-flow LVAD is attempted to assess the change in hemodynamic characteristics inside the heart by using ANSYS FLUENT. Simulations have been carried out for both the diastolic and systolic phases. The obtained results are then compared with the fluidics of a healthy left heart without any support of LVAD. The following observations are drawn from the investigation:

- Significant change in hemodynamics is noticed after LVAD implantation; the heart loses its rhythmic blood wave (pulsatile flow output).
- Major change in blood flow dynamics is noticed at the aorta for both the cardiac phases:
 - During diastole: A flow bisection of the incoming blood stream from the pump through the graft is noticed at the ascending aorta. Some part of the flow stream travels back toward the aortic root (a region of flow recirculation is noticed here) while other advances towards the descending aorta.

- During systole: A major part of blood flow is contributed by the pump, due to which a void (without any flow) is noticed at the central region of ascending aorta. This flow characteristic hugely deviates from the actual blood flow in native heart (without any LVAD).
- The change in hemodynamics is not only observed in the left heart but also noticed in the blood pump. The flow characteristics due to the tubular assumption of pump inlet are observed to be very regular and uniform compared to the realistic case (inlet from ventricle through inflow cannula). These deviations in the flow field may raise discrepancies in many other dependent results.
- Implantation of LVAD also elevates the shear on the heart wall. In particular, high WSS spots are noticed near the ascending and arch region of the aorta.

Above mentioned observations provide information about critical zones to be monitored in case of a patient-specific heart with LVAD. Multiple future studies with different heart geometries after relaxing limitations of present work may lead towards development of a predicting tool prior to implant of LVAD in human heart.

Acknowledgements This research work was supported by the Ministry of Human Resource Development (MHRD) and Indian Council of Medical Research (ICMR) under the IMPRINT scheme (award number 3-18/2015-TSI).

Declarations

Conflict of interest The authors declare no competing interests.

References

1. Ambrosy AP, Fonarow GC, Butler J et al (2014) The global health and economic burden of hospitalizations for heart failure: lessons learned from hospitalized heart failure registries. *J Am Coll Cardiol* 63(12):1123–1133
2. Trivedi JR, Cheng A, Singh R, Williams ML, Slaughter MS (2014) Survival on the heart transplant waiting list: impact of continuous flow left ventricular assist device as bridge to transplant. *Ann Thorac Surg* 98:830–834
3. InformedHealth.org [Internet]. Cologne, Germany: Institute for Quality and Efficiency in Health Care (IQWiG); 2006-. Types of heart failure. 2018 Jan 25. Available from: <https://www.ncbi.nlm.nih.gov/books/NBK481485/>
4. Sen A, Larson JS, Kashani KB et al (2013) Mechanical circulatory assist devices: a primer for critical care and emergency physicians. *Crit Care* 20(1):153
5. Stöhr EJ, McDonnell BJ, Colombo PC, Willey JZ (2019) Cross-Talk proposal: blood flow pulsatility in left ventricular assist device patients is essential to maintain normal brain physiology. *J Physiol* 597:353–356
6. Pozzi M, Giraud R, Tozzi P et al (2015) Long-term continuous-flow left ventricular assist devices (LVAD) as bridge to heart

- transplantation. *J Thorac Dis* 7(3):532–542. <https://doi.org/10.3978/j.issn.2072-1439.2015.01.45>
7. Cheng A, Williamitis CA, Slaughter MS (2014) Comparison of continuous-flow and pulsatile-flow left ventricular assist devices: is there an advantage to pulsatility? *Ann Cardiothorac Surg* 3(6):573–581. <https://doi.org/10.3978/j.issn.2225-319X.2014.08.24>
 8. Kannojiya V, Das AK, Das PK (2021) Comparative assessment of different versions of axial and centrifugal LVADs: a review. *Artif Organs Early Access*. <https://doi.org/10.1111/aor.13914>
 9. Su B, Kabinejadian F, Phang HQ, Kumar GP, Cui F, Kim S et al (2015) Numerical modeling of intraventricular flow during diastole after implantation of BMHV. *PLoS ONE* 10(5):e0126315. <https://doi.org/10.1371/journal.pone.0126315>
 10. Seo JH, Vedula V, Abraham T, Lardo AC, Dawoud F, Luo H, Mittal R (2014) Effect of the mitral valve on diastolic flow patterns. *Phys Fluids* 26:121901
 11. Lantz J, Gupta V, Henriksson L, Karlsson M, Persson A, Carlhäll CJ, Ebberts T (2019) Impact of pulmonary venous inflow on cardiac flow simulations: comparison with in vivo 4d flow MRI. *Ann Biomed Eng* 47(2):413–424
 12. Lantz J, Henriksson L, Persson A, Karlsson M, Ebberts T (2016) Patient-specific simulation of cardiac blood flow from high-resolution computed tomography. *J Biomech Eng* 138(12):121004-1–9. <https://doi.org/10.1115/1.4034652>
 13. Jahanzamin J, Fatouraei N, Moghaddam AN (2019) Effect of turbulent models on left ventricle diastolic flow patterns simulation. *Comput Methods Biomech Biomed Eng* 22(15):1229–1238
 14. Wiegmann L, Boes S, de ZeLicourt DD, Thamsen B, Schmid Daners M, Meboldt M et al (2018) Blood pump design variations and their influence on hydraulic performance and indicators of hemocompatibility. *Ann Biomed Eng* 46:417–428
 15. Heck LM, Yen A, Snyder TA, O'Rear EA, Papavassiliou V (2017) Flowfield simulations and hemolysis estimated for the food and drug administration critical path initiative centrifugal blood pump. *Artif Organs* 41:E129–E140
 16. Kannojiya V, Das AK, Das PK (2020) Numerical simulation of centrifugal and hemodynamically levitated LVAD for performance improvement. *Artif Organs* 44(2):E1–E19
 17. Yu J, Zhang X (2016) Hydrodynamic and hemolysis analysis on distance and clearance between impeller and diffuser of axial blood pump. *J Mech Med Biol* 16(1):1650014
 18. Good BC, Manning KB (2020) Computational modeling of the food and drug administration's benchmark centrifugal blood pump. *Artif Organs* 44(7):E263–E276
 19. Karmonik C, Partovi S, Loebe M, Schmack B, Weymann A, Lumsden AB, Karck M, Ruhparwar A (2014) Computational fluid dynamics in patients with continuous-flow left ventricular assist device support show hemodynamic alterations in the ascending aorta. *J Thorac Cardiovasc Surg* 147(4):1326–1333. e1. <https://doi.org/10.1016/j.jtcvs.2013.09.069>
 20. Aliseda A, Chivukula VK, Megah P, Prisco AR, Beckman JA, Garcia GJ, Mokadam NA, Mahr C (2017) LVAD outflow graft angle and thrombosis risk. *ASAIO J Jan/Feb* 63(1):14–23. <https://doi.org/10.1097/MAT.0000000000000443>
 21. Kasinpila P, Kong S, Fong R, Shad R, Kaiser AD, Marsden AL, Woo YJ, Hiesinger W (2020) Use of patient-specific computational models for optimization of aortic insufficiency after implantation of left ventricular assist device. *J Thorac Cardiovasc Surg* 15:S0022–5223(20)31173–9. doi: <https://doi.org/10.1016/j.jtcvs.2020.04.164>.
 22. Aigner P, Schweiger M, Fraser K et al (2020) Ventricular flow field visualization during mechanical circulatory support in the assisted isolated beating heart. *Ann Biomed Eng* 48:794–804. <https://doi.org/10.1007/s10439-019-02406-x>
 23. Wang Y, Wang J, Peng J, Huo M, Yang Z, Giridharan GA, Luan Y, Qin K (2021) Effects of a short-term left ventricular assist device on hemodynamics in a heart failure patient-specific aorta model: a CFD study. *Front Physiol* 12:1518
 24. Ghodrati M, Maurer A, Schlöglhofer T, Khienwad T, Zimpfer D, Beitzke D, Zonta F, Moscato F, Schima H, Aigner P (2020) The influence of left ventricular assist device inflow cannula position on thrombosis risk. *Artif Organs* 44(9):939–946
 25. Su B, Wang X, Kabinejadian F, Chin C, Le TT, Zhang JM (2019) Effects of left atrium on intraventricular flow in numerical simulations. *Comput Biol Med* 106:46–53
 26. Kannojiya V, Das AK, Das PK (2020) Proposal of hemodynamically improved design of an axial flow blood pump for LVAD. *Med Biol Eng Comput* 58(2):401–418
 27. Giersiepen M W L J, Opitz R, Reul H (1990) Estimation of shear stress-related blood damage in heart valve prostheses in vitro comparison of 25 aortic valves. *Int J Artif Organs* 13(5):300–306
 28. Taskin ME, Fraser KH, Zhang T, Gellman B, Fleischli A, Dasse KA et al (2010) Computational characterization of flow and hemolytic performance of the UltraMag blood pump for circulatory support. *Artif Organs* 34:1099–1113
 29. Faghig MM, Sharp MK (2016) Extending the power-law hemolysis model to complex flows. *J Biomech Eng* 138:124504–124511
 30. Caruso MV, Gramigna V, Rossi M, Serraino GF, Renzulli A, Fragomeni G (2015) A computational fluid dynamics comparison between different outflow graft anastomosis locations of left ventricular assist device (LVAD) in a patient-specific aortic model. *Int J Numer Method Biomed Eng*. 31(2)
 31. Goldstein DJ, Oz MC, Rose EA (1998) Implantable left ventricular assist devices. *N Eng J Med* 339(21):1522–1533
 32. Dahl SK, Thomassen E, Hellevik LR et al (2012) Impact of pulmonary venous locations on the intra-atrial flow and the mitral valve plane velocity profile. *Cardiovasc Eng Tech* 3:269–281
 33. Sun A, Zhao B, Ma K, Zhou Z, He L, Li R, Yuan C (2017) Accelerated phase contrast flow imaging with direct complex difference reconstruction. *Magn Reson Med* 77:1036–1048
 34. Ahmad Bakir A, Al Abed A, Stevens MC, Lovell NH, Dokos S (2018) A multiphysics biventricular cardiac model: simulations with a left-ventricular assist device. *Front Physiol*. 9:1259. <https://doi.org/10.3389/fphys.2018.01259> (Published 2018 Sep 11)
 35. Doost SN, Zhong L, Su B, Morsi YS (2016) The numerical analysis of non-Newtonian blood flow in human patient-specific left ventricle. *Comput Methods Programs Biomed* 127:232–247
 36. Kannojiya V, Das AK, Das PK (2021) Simulation of blood as fluid: a review from rheological aspects. *IEEE Rev Biomed Eng* 14:327–341
 37. Khan M, Sardar H, Gulzar MM, Alshomrani AS (2018) On multiple solutions of non-Newtonian Carreau fluid flow over an inclined shrinking sheet. *Results Phys* 8:926–932
 38. Cho YI, Kensey KR (1991) Effects of the non-Newtonian viscosity of blood on flows in a diseased arterial vessel Part 1: Steady flows. *Biorheology* 28(3–4):241–262. <https://doi.org/10.3233/bir-1991-283-415>
 39. Johnston BM, Johnston PR, Corney S, Kilpatrick D (2004) Non-Newtonian blood flow in human right coronary arteries: steady state simulations. *J Biomech* 37:709–720
 40. Mamun K, Rahman MM, Akhter MN, Ali M (2006) Physiological non-Newtonian blood flow through single stenosed artery. *AIP Conf Proc*. 2006:1754, Art. no. 040001
 41. Grigoriadis GI, Sakellarios AI, Kosmidou I, Naka KK, Ellis C, Michalis LK, Fotiadis DI (2020) Wall shear stress alterations at left atrium and left atrial appendage employing abnormal blood velocity profiles. *Annu Int Conf IEEE Eng Med Biol Soc*. 2565–2568.
 42. Dean Vucinic TY, Aksenov AA (2016) Human heart blood flow simulations based on CFD *Int. J Fluid Heat Transfer* 1:15–34

43. Sang X, Zhou X (2017) Investigation of hydraulic performance in an axial-flow blood pump with different guide vane outlet angle. *Adv Mech Eng* 9(8):1–11
44. Bensalah ZM, Bollache E, Kachenoura N et al (2012) Ascending aorta backward flow parameters estimated from phase-contrast cardiovascular magnetic resonance data: new indices of arterial aging. *J Cardiovasc Magn Reson* 14:P128. <https://doi.org/10.1186/1532-429X-14-S1-P128>
45. Leeuwenburgh BP, Helbing WA, Steendijk P, Schoof PH, Baan J (2003) Effects of acute left ventricular unloading on right ventricular function in normal and chronic right ventricular pressure-overloaded lambs. *J Thorac Cardiovasc Surg* 125:481–490
46. Callaghan FM, Grieve SM (2018) Normal patterns of thoracic aortic wall shear stress measured using four-dimensional flow MRI in a large population. *Am J Physiol Heart Circ Physiol* 315(5):H1174–H1181. <https://doi.org/10.1152/ajpheart.00017.2018>
47. De Wachter DS, Verdonck PR, Verhoeven RF, Hombrouckx RO (1996) Red cell injury assessed in a numerical model of a peripheral dialysis needle. *ASAIO J* 42:524–529
48. Etlí M, Canbolat G, Karahan O et al (2021) Numerical investigation of patient-specific thoracic aortic aneurysms and comparison with normal subject via computational fluid dynamics (CFD). *Med Biol Eng Comput* 59:71–84
49. Sacco F, Paun B, Lehmkuhl O, Iles TL, Iaizzo PA, Houzeaux G, Vázquez M, Butakoff C, Aguado-Sierra J (2018) Left ventricular trabeculations decrease the wall shear stress and increase the intra-ventricular pressure drop in CFD simulations. *Front Physiol* 30(9):458
50. Lopes D, Puga H, Teixeira JC, Teixeira SF (2019) Influence of arterial mechanical properties on carotid blood flow: comparison of CFD and FSI studies. *Int J Mech Sci* 160:209–218
51. Torii R, Wood NB, Hadjiloizou N, Dowsey AW, Wright AR, Hughes AD et al (2009) Fluid–structure interaction analysis of a patient-specific right coronary artery with physiological velocity and pressure waveforms. *Commun Numer Meth En* 25(5):565–580

Publisher's Note Springer Nature remains neutral with regard to jurisdictional claims in published maps and institutional affiliations.



Arup Kumar Das is an associate professor in the Mechanical and Industrial Engineering Department, IIT Roorkee, India. His research interest focuses on CFD, multiphase fluid dynamics, and heat transfer.



Prasanta Kumar Das is a professor in the Mechanical Engineering Department, IIT Kharagpur, India. His research interest focuses on single- and multiphase fluid dynamics, heat transfer, and thermal engineering.



Vikas Kannojiya is a research scholar in the Mechanical and Industrial Engineering Department, IIT Roorkee, India. His research focuses on bio-fluidics, medical device design, and CFD.